Paper

VARIATIONS IN ASTRONAUT RADIATION EXPOSURE DUE TO ANISOTROPIC SHIELD DISTRIBUTION

John W. Wilson,* John E. Nealy,* James S. Wood,† Garry D. Qualls,†
William Atwell,‡ Judy L. Shinn,§ and Lisa C. Simonsen§

Abstract—**The dose incurred in an environment generated by extraterrestrial space radiations within an anisotropic shield distribution depends on the orientation of the astronaut's body relative to the shield geometry. The fluctuations in exposure of specific organ sites due to astronaut re-orientation are found to be a factor of 2 or more in a typical space habitation module and typical space radiations. An approximation function is found that overestimates astronaut exposure in most cases studied and is recommended as a shield design guide for future deep space missions.**

Health Phys. 69(1):34–45; 1995

Key words: exposure, radiation; radiation, atmospheric; shielding; risk analysis

INTRODUCTION

THERE ARE many uncertainties that enter into estimates of biological risk to astronauts in deep space that must be managed to ensure astronaut radiation exposure risk in future missions does not exceed acceptable limits. These uncertainties are from several sources: (1) models for the external environment; (2) modification of the external environment by shielding materials; (3) the shielding geometry models; (4) computational methods for estimating the internal environment of the spacecraft; (5) interaction of the interior environment with the human body; (6) the body geometry; (7) computational procedures for relating the internal environment to exposure of specific tissues; and (8) the biological response to specific tissue exposures.

Environmental uncertainties arise from the galactic cosmic ray (GCR) models used and the unpredictable nature of solar particle events (SPE). Improvements in GCR models are in progress (Badhwar et al. 1993), but SPE exposures will remain unpredictable into the foreseeable future (Smart and Shea 1989). A maximum observed SPE fluence event is usually used for design purposes (Wilson et al. 1993a). This is not to say that these fluence levels may not someday be exceeded but rather that no observed event has exceeded them in the past.

The uncertainty in the shielding properties of materials is not accurately known for the high charge and energy (HZE) components. Significant uncertainty is known to result from the choice of nuclear models (Wilson et al. 1987). Uncertainty in shielding properties for the biologically most significant components on the order of 200% has been estimated on the basis of physical limits on reaction mechanisms (Townsend et al. 1992). A further computational uncertainty caused by assuming that nuclear cross sections for HZE fragmentation are energy independent adds an additional 50% uncertainty (Shinn et al. 1992). It is impractical to fully represent the geometry of the spacecraft structure, even on current software systems and computers. Furthermore, the geometry varies throughout the mission as expendables are consumed (Nealy et al. 1991). In principal, Monte Carlo methods could match boundary conditions but are not operable in an integrated engineering software environment. In practice, the three-dimensional aspects of the solution to the Boltzmann equation are simplified and boundary conditions are never exactly matched (Wilson and Khandelwal 1974; Wilson et al. 1991). However, conservative methods are normally employed that rarely cause significant errors (Wilson and Khandelwal 1974). The interior environment is rarely evaluated at more than a few specific locations so that the boundary flux (including leakage) at the surface of the astronaut's body is never exactly specified (Wilson and Khandelwal 1974; Atwell et al. 1991). There is further uncertainty in the interaction with the body tissues (Schimmerling 1992a) and specification of the body geometry (Atwell et al. 1991; Billings and Yucker 1973). Finally, the biological response to many of the environmental components is largely unknown (NCRP 1989; Schimmerling 1992b). Clearly, all of these factors must be dealt with in a consistent fashion to ensure astronaut safety in future deep-space missions. In the present report we endeavor to consider uncertainty associated with astronaut geometric factors (specifically, astronaut orientation within the space vehicle living quarters).

* NASA Langley Research Center, Hampton, VA 23681-0001; † Flight Mechanics Control, Inc., Hampton, VA 23669; ‡ Rockwell International, Space Transportation Systems Division, Houston, TX 77058; § NASA Langley Research Center, Hampton, VA 23681-0001.

(*Manuscript received* 3 *November* 1993; *revised manuscript received* 28 *December* 1994, *accepted* 7 *February* 1995)

0017-9078/95/$3.00/0

If the radiation fields to which the astronaut is exposed are isotropic, then the exposure of specific organs is independent of the astronaut orientation. Radiations within the geomagnetic field are anisotropic, since particle motion is strongly affected by the local magnetic field direction. Even outside the geomagnetic field where galactic and solar cosmic rays are nearly isotropic (SPEs show some anisotropy in the first half hour of the event and rapidly approach isotropy which persists several hours or days), the astronaut is enclosed within a large spacecraft of a complicated geometric shape in which the resulting interior radiation fields are highly anisotropic. The radiation anisotropy is related to the distribution of material about the radiation field point. In the present report, we suggest a design criteria for estimating shield requirements within a typical spacecraft geometry for isotropic space radiations which includes no less than 85–90% of the total exposure in deep space. A similar criteria for the anisotropic phase of an SPE or geomagnetically trapped radiations is beyond the scope of the present study.

As a practical example, we consider a representative crew living module as illustrated in Fig. 1. The module configuration is defined by a computer-aided design (CAD) model developed by Langley Research Center based on early Space Station *Freedom* layouts and includes racks, end plates, windows, utility raceways, and the pressure vessel walls. Appropriate nominal densities have been assigned to each of the constituents. Three interior points along the centerline have been chosen for dose analysis: (1) in the end (windowed) section least protected by inherent shielding; (2) near the geometric center where maximum shielding exists; and (3) at the opposite end location where intermediate shielding exists. These points will be referred to as A, B, and C, respectively. Directional thickness data prescribed in a three-dimensional reference frame must be used to examine the effects of differing orientations at a given location in the spacecraft. Fig. 2 shows such directional thickness patterns for the specified target points in the CAD-modeled habitation module. It is apparent that the central location offers greatest protection, while positions near the end walls are associated with smaller thickness values in directions facing away from the center region. Shadowing due to utility raceways, racks, and plates is also prominent in the illustrations. The directional patterns are based on thicknesses along 1,922 rays evenly distributed about the target point with respect to solid angle.

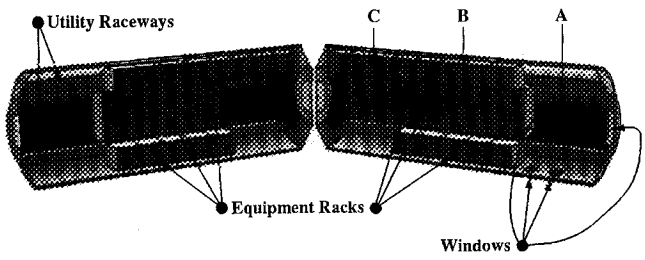

Fig. 1. Computer-aided design model of space station Freedom habitation module derivative.

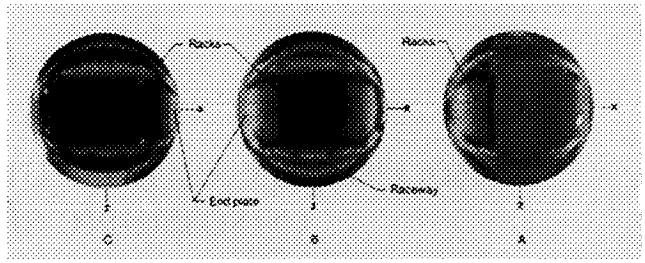

Fig. 2. Directional thickness patterns for three interior locations in the CAD-modeled habitation module. (Relative thickness increases as gray scale progresses from light to dark.)

The NASA computerized anatomical man (CAM) model (Billings and Yucker 1973) is used to define the astronaut geometry. Directional thickness patterns for the selected human body target points are shown in Fig. 3. The pattern for the skin at a central chest location exemplifies the contrast between the most shielded directions and the most exposed directions, which results in two approximate hemispherical patterns (light in front and dark in back). The distribution about the right-eye location also indicates a large solid angle of high exposure, but noticeable asymmetry exists because of the off-axis position of this target. The thyroid and esophageal distributions are indicative of intermediate self-shielding locations, and the intestine point represents that for which most self-shielding is available. The CAM model distributions are derived from a 512-ray pattern, and while the directional resolution is not as good as for the habitat module, the thickness patterns are generally defined well enough to make important features readily identifiable. The patterns in Fig. 3 are oriented so that the head location is toward the top of the direction sphere; the frontal direction is indicated by the position of the solid angle for which least shielding occurs.

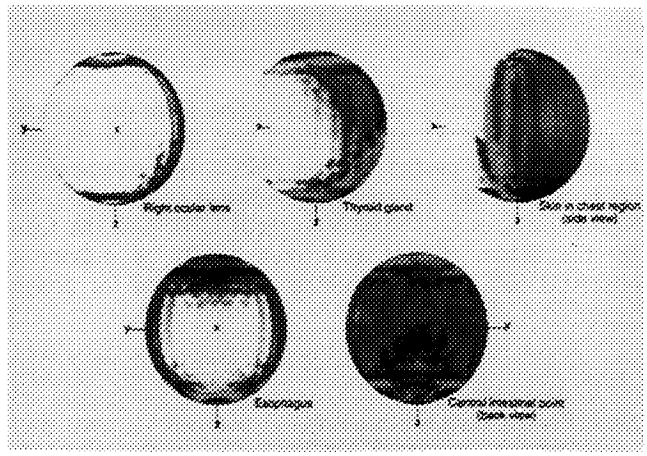

Fig. 3. Directional thickness patterns for selected CAM model body target points. (Relative thickness increases as gray scale progresses from light to dark.)

It is clear that the exposure at a location in the astronaut's body depends on the distribution of the vehicle's structural mass and the astronaut's body mass about the exposure point. How the two mass distributions combine depends on the orientation of the astronaut relative to the vehicle. The importance of this orientation on evaluating astronaut exposure is the object of the current study.

DOSE WITHIN CONVEX REGIONS

It can be shown (Wilson and Khandelwal 1974) that the dose from proton or ion exposure within a convex region can be approximated (conservatively) by

$$D(\vec{x}) = \iint R[E, t_x(\vec{\Omega})]\, \Phi(E, \vec{\Omega})\, d\vec{\Omega}\, dE, \qquad (1)$$

where $R(E, z)$ is the solution for the normally incident beam of particles of energy E in slab geometry at a depth z, and $\Phi(E, \vec{\Omega})$ is the fluence density of ions of energy E moving in direction Ω. The error in eqn (1) is second order in the ratio of beam divergence to radius of curvature and is typically a few percent for space radiations. The distribution of shield material about the dose point $\vec{x}$ is defined by the areal density distribution $t_x(\vec{\Omega})$.

In the case of a mono directional beam, the dose according to eqn (1) is

$$D_{\vec{\Omega}_B}(\vec{x}) = \int \Phi(E) R[E, t_x(\vec{\Omega}_B)]\, dE, \qquad (2)$$

where $\vec{\Omega}_B$ is the radiation direction. If we randomly reorient the body relative to the direction of irradiation, the dose fluctuates at $\vec{x}$ according to the distribution of areal density about $\vec{x}$ given by $f_x(t)dt$. Note that $f_x(t)dt$ is the probability for an arbitrarily chosen direction that the shield thickness lies between t and $t + dt$. The NASA CAM model has been used to provide thickness cumulative distribution functions (cdfs) and probability density functions (pdfs) for selected human body exposure locations. The body target points for this study have been chosen to represent varying degrees of body self-shielding (that is, from lightly shielded body points to heavily shielded ones). In order of increasing amount of self-shielding, the five selected points are located in (1) skin in chest region; (2) right ocular lens; (3) thyroid gland; (4) esophagus; and (5) central intestinal point. The respective thickness distributions are shown in Fig. 4 (a)-(e). The peak value of the pdf at each body target point is an indicator of relative effective self-shielding. Note that the semilogarithm plots of Fig. 4 allow a simple judgement of area under the curve to relate to cumulative distributions by using the quantity $tf_x(t)$. The mean dose for all orientations is evaluated by using a code developed by Shinn et al. (1990) as

$$\begin{aligned} \overline{D}_x &= \iint \Phi(E) R[E, t_x(\vec{\Omega}_B)]\, d\vec{\Omega}_B\, dE \\ &= \iint \Phi(E) R(E, t) f_x(t)\, dt\, dE. \end{aligned} \qquad (3)$$

The standard deviation of dose, σ_o is given by

$$\sigma_o^2 = \iint [\Phi(E) R(E, t)]^2 f_x(t)\, dt - \overline{D}_x^2. \qquad (4)$$

In general, the exposure fluctuations are not well represented by normal statistics, and the standard deviation has no clear meaning except in the general sense that it is a measure of dose variation (Wilson et al. 1993b).

ASTRONAUT EXPOSURE WITHIN A SPACECRAFT

In the case of isotropic radiation exposure, one may rewrite eqn (1) as

$$D(\vec{x}) = \int \Phi(E) dE \int R[E, t_x(\vec{\Omega})]\, d\vec{\Omega}, \qquad (5)$$

for which the fractional solid angle distribution may be introduced as

$$D(\vec{x}) = 4\pi \int \Phi(E)\, dE \int_0^\infty R(E, t) f_x(t)\, dt, \qquad (6)$$

where $f_x(t)dt$ is the solid angle fraction with $t_x(\vec{\Omega})$ lying between t and $t + dt$. Note $f_x(t)$ is related to the directional thickness distribution of the previous section. The dose in the center of a sphere is found by taking $f_x(t)$ to be $\delta(t - r)$ so that

$$D_{sp}(r) = 4\pi \int \Phi(E)\, dE\, R(E, r), \qquad (7)$$

from which the dose at a point $\vec{x}$ in arbitrary geometry can be written as

$$D(\vec{x}) = \int D_{sp}(t) f_x(t)\, dt. \qquad (8)$$

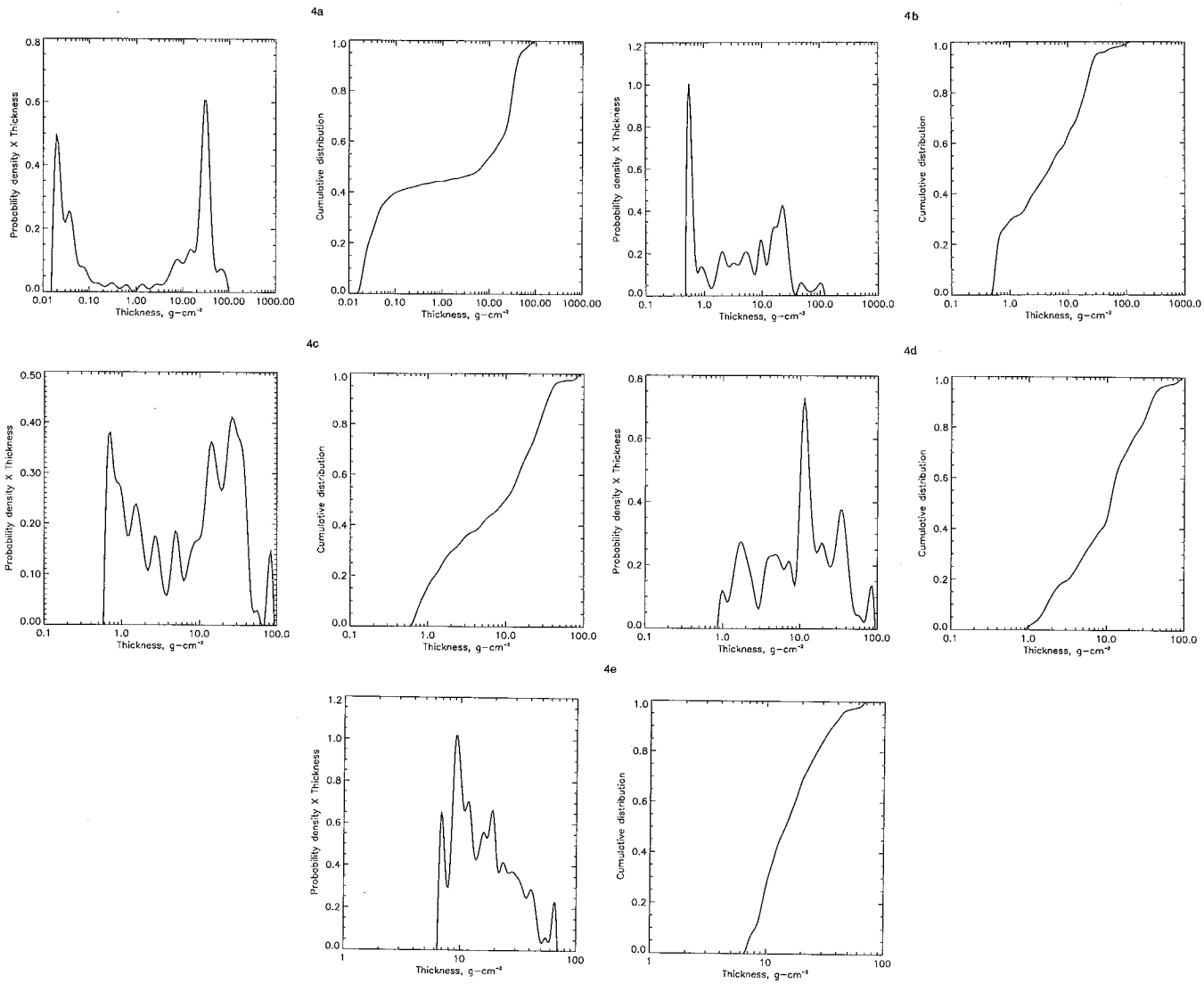

Fig. 4. Thickness distribution functions obtained from the NASA computerized anatomical man model for five body target points located in the (a) skin in chest region; (b) right ocular lens; (c) thyroid gland; (d) esophagus; and (e) central intestinal point.

The error generated by eqn (5) is second order in the ratio of beam divergence to radius of curvature of the exposed object and is always conservative (Wilson and Khandelwal 1974). Note that eqn (7) approximates the dose in the center of a sphere by the dose in a slab for which all the radiation is incident normally on the exterior surface. Obviously, such an assumption is conservative since leakage at the sphere boundary is underestimated in slab geometry but approaches the slab as the sphere radius becomes large (Wilson and Khandelwal 1974).

If the convex body is allowed to rotate to a new position defined by a colatitude and azimuth, then the integral of eqn (1) becomes

$$D(\vec{x}) = \iint R\{E, t_x[R_y(\theta)R_z(\phi)\vec{\Omega}]\}\, \Phi(E, \vec{\Omega})\, d\vec{\Omega}\, dE \qquad (9)$$

where $R_y(\theta)$ and $R_z(\phi)$ are rotation operators (Wilson 1968). The average exposure for all orientations is then

$$\bar{D}(\vec{x}) = \frac{1}{4\pi}\iiint R\{E, t_x[R_y(\theta)R_Z(\phi)\vec{\Omega}]\} \cdot \Phi(E, \vec{\Omega})\, d\vec{\Omega}\, d\vec{\Omega}'\, dE \qquad (10)$$

$$= \iint R(E, t)\, \Phi(E, \vec{\Omega})\, d\vec{\Omega} f_x(t)\, dE\, dt,$$

which shows that a randomly rotating body exposure is equivalent to assuming the omnidirectional flux is isotropic as intuition dictates.

Suppose a region b is to be protected by enclosing it within a region s; then the dose at a point $\vec{x}$ within b is

$$D(\vec{x}) = \int\int R[E, t_s(\vec{\Omega}) + t_b(\vec{\Omega})]\, \Phi(E, \vec{\Omega})\, dE\, d\vec{\Omega}, \quad (11)$$

where we assume the body and shield are constructed of the same (or equivalent) material. Otherwise, $R(E, t)$ must be replaced by the more complicated functions derived as buildup factors in multilayered media (Wilson and Khandelwal 1976; Wilson et al. 1991). If the body is randomly rotated within the shield, then

$$D(\vec{x}) = \int\int R[E, t_s(\vec{\Omega}) + t_b] f_b(t_b) dt_b \Phi(E, \vec{\Omega})\, dE\, d\vec{\Omega}, \quad (12)$$

which may be reduced for isotropic exposure to

$$D(\vec{x}) = 4\pi \int\int R(E, t_s + t_b) f_s(t_s) f_b(t_b) \Phi(E) dE\, dt_b\, dt_s$$
$$= \int D_{sp}(t) \int f_s(\tau) f_b(t - \tau)\, dt\, d\tau, \quad (13)$$

where $D_{sp}(t)$ is the dose in the center of a sphere of radius t. Note that from eqn (13) we define a combined areal density distribution function as

$$f_{sb}(t) = \int f_s(\tau) f_b(t - \tau)\, d\tau, \quad (14)$$

which is valid for a randomly rotating inner body shielded by a distribution $f_s(t_s)$ in an isotropic environment. Clearly, eqn (13) is the average dose over rotations and the associated distribution function is given by eqn (14).

It is shown in Appendix A that for a shielded region of average thickness $\langle t \rangle$ that the maximum protection is provided by a spherically symmetric shield (that is, the radius is $t = \langle t \rangle$ and the thickness variance is zero). We will now further examine this dependence on the thickness variance.

Although the areal density distribution functions contain no specific information on orientation, we may nonetheless use them to provide an upper and lower bound on exposure. The dose within a body in a shielded region is given by eqn (11). If the body is reoriented by rotations (θ, ϕ) then

$$D(\vec{x}) = \int\int\int R\{E, t_s(\vec{\Omega}) + t_b[R_y(\theta) R_z(\phi) \vec{\Omega}]\}\, \Phi(E, \vec{\Omega}) dE\, d\vec{\Omega}. \quad (15)$$

Clearly, $D(\vec{x})$ depends on the orientation angles. For an isotropic environment as is usually found in deep space,

$$D(\vec{x}) = \int D_{sp}\{t_s(\vec{\Omega}) + t_b[R_y(\theta) R_z(\phi) \vec{\Omega}]\}\, d\vec{\Omega}. \quad (16)$$

For a given set of angles (θ,ϕ) there is a unique areal density distribution for which

$$D(\vec{x}) = \int D_{sp}(t) f_{sb}(t, \theta, \phi)\, dt. \quad (17)$$

Clearly, the minimum exposure occurs when θ and ϕ are chosen to best approach spherical symmetry and maximum exposure when the maximum deviation from spherical symmetry occurs. It is obvious that the average thickness $(t_s + t_b)$ is independent of orientation, but the thickness standard deviation σ could change considerably. If σ approaches zero, then $D(\vec{x}) \approx D_{sp}(\bar{t})$; a large σ yields

$$D(\vec{x}) = D_{sp}(\bar{t}) \left(1 + \frac{1}{2}\alpha^2(\sigma)^2 + \cdots\right), \quad (18)$$

showing the minimum variance to be the optimum configuration and the maximum variance to be the worst-case exposure as expected.

As mentioned above, the areal density distributions contain no specific directional information. However, we may seek combinations of areal densities for which the variance is either minimized or maximized corresponding to bounds on the body exposure due to orientation. As was shown earlier, the average over all orientations is given by the convolution as

$$\bar{f}_{sb}(t) = \frac{1}{4\pi} \int f_{sb}(t, \theta, \phi)\, d\vec{\Omega} = \int_o^t f_s(\tau) f_b(t - \tau)\, d\tau. \quad (19)$$

The maximum variance combination F_u is found by matching the solid angles with least thickness and the solid angles with maximum thickness for each of the two regions. Obviously, this assumes high angular correlation of the two thickness distributions. Thus, F_u is the combined solid angle fraction with thickness less than $t = t_b + t_s$, where t_b and t_s are given as solutions of

$$F_b(t_b) = F_u(t) \quad (20)$$

$$F_s(t_s) = F_u(t), \quad (21)$$

and $F_b(t_b)$ and $F_s(t_s)$ are the cumulative distributions for the body and shield. Similarly, assuming good angular correlation, the minimum variance combination $F_L(t)$ is found from

$$F_b(t_b) = 1 - F_L(t) \quad (22)$$

$$F_s(t_s) = F_L(t), \quad (23)$$

where $t = t_s + t_b$ as before. Note that the upper and lower limits given by eqns (20) to (23) would correspond most closely to the 3σ limits of a normal distribution (Wilson

et al. 1993b). The mean exposure is given by the convolution in eqn (19).

It is clear in the above constructions that the mean thickness is preserved in each case. The standard deviation of the combined thickness distribution is, however, quite distinct. It can be shown that the standard deviation of thickness for a randomly rotated, inner body is

$$\sigma_{sb} = (\sigma_s^2 + \sigma_b^2)^{1/2}, \tag{24}$$

corresponding to the distribution of eqn (19) associated with average dose over all rotations. The standard deviation of the combined mass distribution for maximum exposure given by eqns (20) and (21) is

$$\sigma_{sb} = \sigma_s + \sigma_b. \tag{25}$$

The minimum exposure standard deviation is given as

$$\sigma_{sb} = |\sigma_s - \sigma_b| \tag{26}$$

corresponding to eqns (22) and (23). As an example of the importance of fluctuations, we assume the dose attenuation function is an exponential in shield thickness and further assume the thickness distributions $f_s(t)$ and $f_b(t)$ are normal, then the mean dose for all orientations is

$$\overline{D} = D_o \exp\left\{-\alpha\left[\bar{t} - (\sigma_s^2 + \sigma_b^2)\frac{\alpha}{2}\right]\right\}, \tag{27}$$

where α^{-1} is the e-folding distance and D_o the unshielded dose. According to the eqns. (25) and (26), the dose standard deviation with orientation is

$$\sigma_o \approx \frac{\overline{D}}{3}\sigma_s\sigma_b\alpha^2\left(1 + \frac{\sigma_s^2\sigma_b^2\alpha^4}{6} + \cdots\right). \tag{28}$$

Although the actual thickness distributions are generally far from normal, the above procedure provides insight into the major factors in dose fluctuations. Clearly, the fluctuations vanish if either the shield or the body mass distribution are spherically symmetric or the attenuation coefficient is small. It should be clear that the above discussion is quite general and applies to dose equivalent and other dosimetric functions as well.

ASTRONAUT IN A HABITAT

We now apply the procedures to the case of an astronaut in the space habitation module. The habitation module used is an early space station *Freedom* design and is shown in Fig. 1. Cost savings projected the use of the space station modules for other space exploration activity such as for a lunar base or a Mars mission. For simplicity, we consider only the three locations in the module denoted by A, B, and C as discussed previously. The thickness distributions about the points are shown in Figs. 2 and 5. For each of the target points, thickness cumulative distribution functions (cdfs) have been deter-

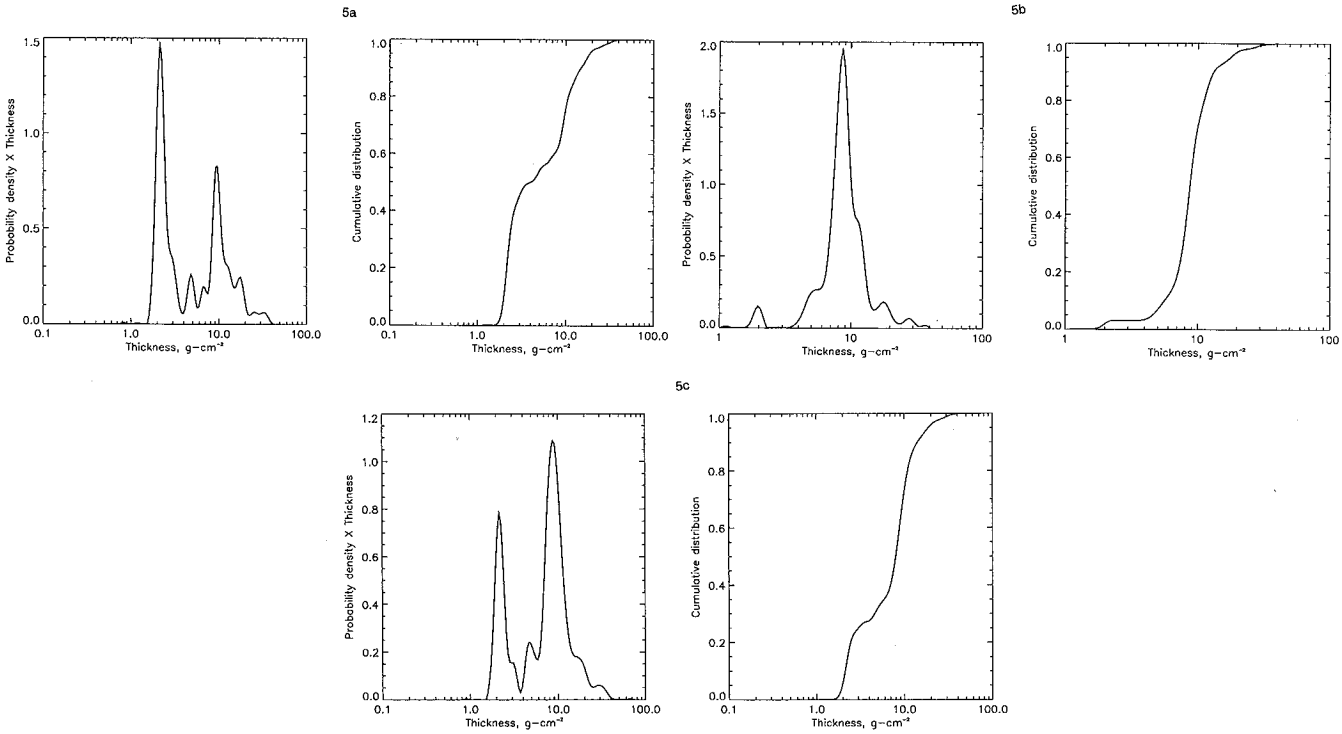

Fig. 5. Thickness distribution functions obtained from the CAD-modeled habitation module for (a) location A; (b) location B; and (c) location C.

mined from which corresponding probability density functions (pdfs) are obtained by differentiation. These distribution functions for the selected interior points in Fig. 1 are shown in Figs. 5 (a–c). Peak values of the pdfs and median (50th percentile) values of the cdfs are indicative of effective shielding at each location. We note that, in the skin thickness distributions (Fig. 4a), the peak pdf value is for small thickness while the medium thickness is near 10 g cm^{-2} and is characteristic of a 2π shadow shield provided by the body torso. It is readily seen that the most protection exists for point B, while the largest exposures are to be expected at point A.

Thickness distributions for the human body within the habitat module may then be constructed for combinations of the cdfs in Figs. 4 and 5 to provide maximum and minimum variance distributions as has been described by eqns (20)–(23). In addition, the distribution corresponding to random orientation may be obtained from the convolution of the module and body pdfs (eqn 19). The set of combined pdfs may then be used in conjunction with appropriate dose-vs.-depth functions to compute the doses to the selected organs at each of the points in the spacecraft structure. Thus, for each combination of body point and position in the module, values for a mean (convolution) dose and a range (minimum, maximum) are found.

We use dose equivalent-vs.-depth functions corresponding to the observed proton spectra for the solar particle events that occurred in February 1956 (very penetrating) and in October of 1989 (moderately penetrating). The event spectra are shown in Fig. 6. The dose equivalent-vs.-depth functions as computed with the Langley BRYNTRN (Wilson et al. 1989; Shinn et al. 1990) code for the observed spectra and the ICRP26 quality factor (NCRP 1989) are shown in Fig. 7. The BRYNTRN code is a deterministic neutron/proton transport code using a simplified (Bertini et al. 1972) nuclear database (Wilson et al. 1989).

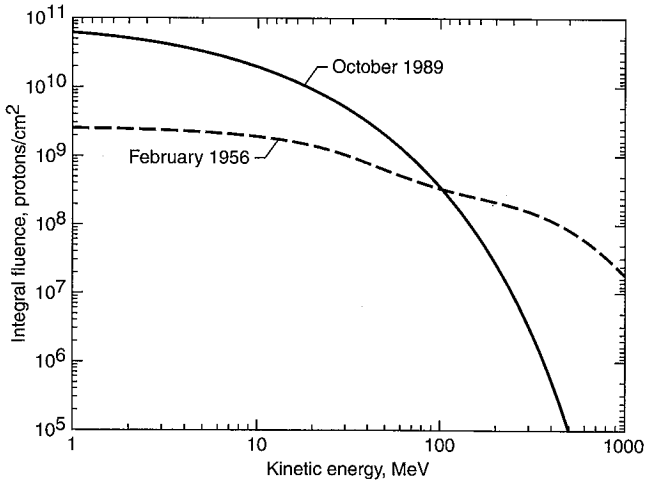

Fig. 6. The integral proton spectra of the February 1956 and October 1989 solar particle events.

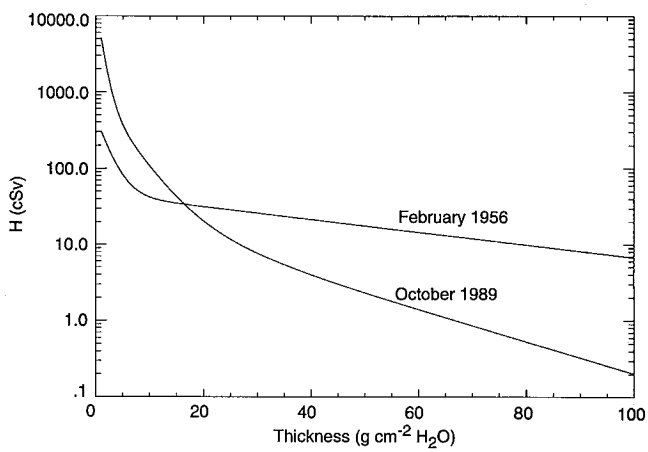

Fig. 7. Computed dose equivalent-vs-depth functions for observed proton flare spectra.

While the dosimetric quantities evaluated from the thickness distribution functions can provide a mean and an absolute range, no direct information regarding variability associated with directional orientation is available. Directional distribution of the internal radiation field can be derived from the thickness distributions at the three designated locations in the habitation module shown in Fig. 2.

Directional dose equivalent patterns projected on the unit sphere are shown in Fig. 8. Note that the gray scale for relative dose equivalent values is the inverse of that for the distributions of thickness. Fig. 8 illustrates dose equivalent patterns for the CAM model body points as computed from the 1989 proton flare dose equivalent-vs.-depth function. Shown are the directional distributions about specific points in the right eye, thyroid, and intestinal track representing points receiving high, moderate, and low exposures, respectively.

The three-dimensional-thickness distributions (illustrated in Figs. 2 and 3) allow one to compute dose equivalent to a specified body target point at a given location in the module for any arbitrary alignment of

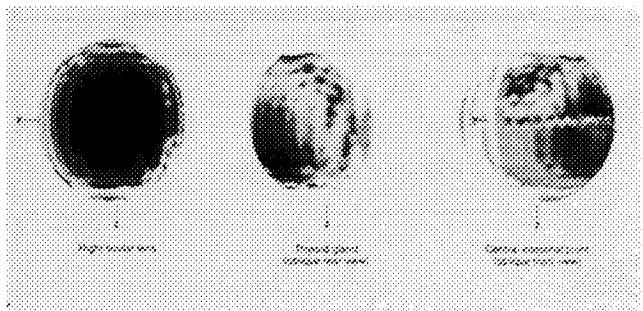

Fig. 8. Dose equivalent patterns for CAM model body points using the 1989 proton flare dose equivalent-vs-depth function. (Relative dose equivalent increases as gray scale progresses from light to dark.)

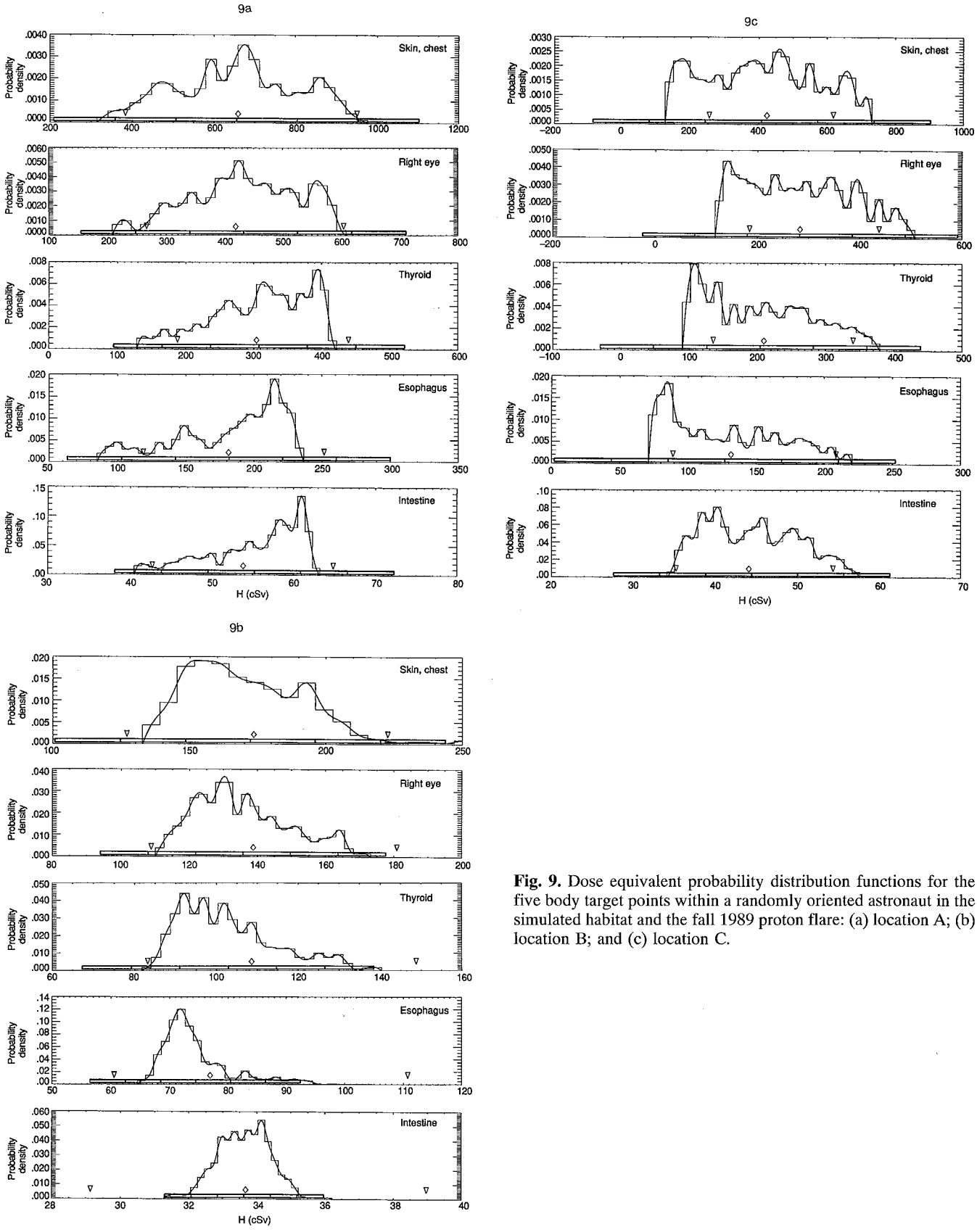

Fig. 9. Dose equivalent probability distribution functions for the five body target points within a randomly oriented astronaut in the simulated habitat and the fall 1989 proton flare: (a) location A; (b) location B; and (c) location C.

relative orientation. Thus, a distribution of dose equivalent values may be obtained that provides not only a mean and an absolute range but also a variance and "practical" range of exposure values. Such information has been obtained in the present study by constructing an algorithm that utilizes a uniform random number distribution to generate statistics on dose equivalent values obtained at various orientations of the body organ points relative to the vehicle orientation (see Appendix B). It was determined (principally by trial and error) that 512 random orientations would provide adequate statistics to define a given distribution of dose values. This procedure was performed for the combinations of selected body points at the three locations in the habitat configuration for the two representative dose equivalent-vs.-depth functions associated with the solar events of October 1989 and February 1956. These results are summarized in Figs. 9 (a–c), and 10 (a–c), which relate to calculations at points A, B, and C in the habitat for the two solar events, respectively. Results for each case are presented as dose equivalent values grouped in 25 bins, along with a spline-fit function through the binned data. The ordinate for each plot is scaled so that the integrated value is unity, and thus represents a probability density in dose equivalent for random orientation. A bar inserted along each abscissa is divided into six segments that indicate 1σ, 2σ, and 3σ values on either side of the calculated mean. Scrutiny of the absolute range values (H_{min}, H_{max})

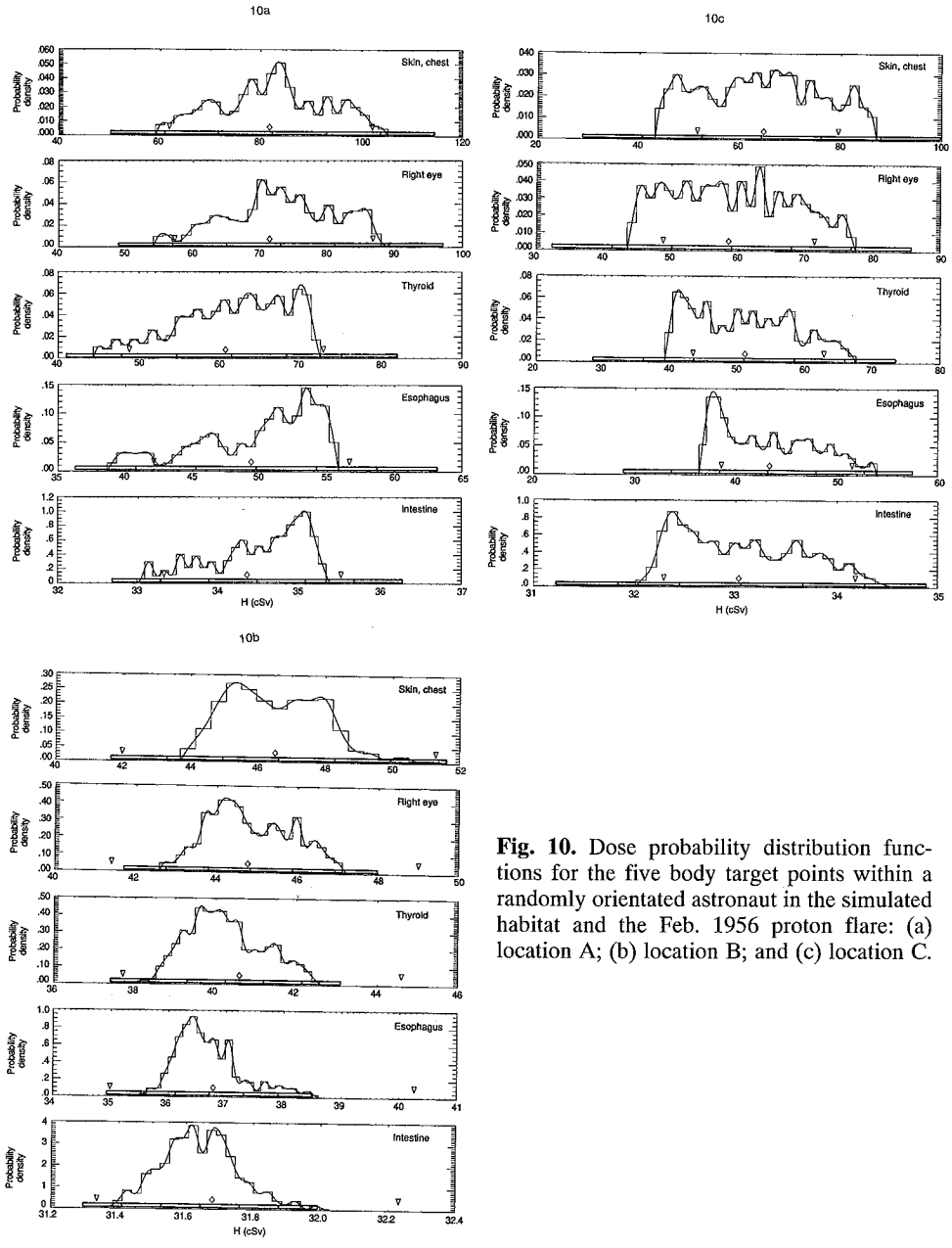

Fig. 10. Dose probability distribution functions for the five body target points within a randomly orientated astronaut in the simulated habitat and the Feb. 1956 proton flare: (a) location A; (b) location B; and (c) location C.

for each case, as computed from the cumulative thickness distributions, has indicated that an approximate "practical" dose equivalent range may be obtained as

$$\frac{\bar{H} + H_{\min}}{2} < H < \frac{\bar{H} + H_{\max}}{2}, \tag{29}$$

where $\bar{H}$ is the mean determined from the convolution integral of the body organ and habitat pdfs. These practical dose equivalent ranges are indicated on the plots as open symbols above the 3σ range bars. The open diamond represents the convoluted value for mean dose equivalent, and the limits of practical range are indicated by the inverted triangles. Note that the practical range is determined by the degree of correlation between the mass distribution of the habitat and the astronaut's body. In most cases, the practical range gives a reasonable approximation to the range of the actual dose equivalent distribution, which may be especially large for some flare spectra. For example, results for exposures at point A due to the fall 1989 spectrum (Fig. 9a) indicate dose equivalent fluctuations by factors of 2 or more about the mean value for the less self-shielded body target points. As may be seen in the results for point B (Fig. 9b), this approximation tends to become conservative when the distribution is sharp (i.e., peaked about a narrow range). The upper limit of the practical range provides a conservative dose equivalent estimate for shield design and is rarely exceeded in application.

Observed differences in the analytic convolution and mean values calculated from the random orientation statistics are attributable both to numerical error in performing the convolution integrations and to the finite number of random orientations included in each case. Clearly, these differences are minor and are indicative of the adequacy of the orientation statistics. In all cases, the variation of dose equivalent with body self-shielding is consistent for the progression between the skin location and the internal intestinal point. The impact of spectral hardness at each habitat location may be seen by comparing Figs. 9 and 10. In particular, one may note the large impact that location in the habitat has on skin and eye dose equivalent for the 1989 flare spectrum, which may be compared with the markedly reduced sensitivity for the much harder February 1956 spectrum.

It is apparent from the results in Figs. 9 and 10 that exposures can be at unacceptable levels without the addition of parasitic shielding. As shielding is added we expect the distribution of dose to narrow as the shield distribution will become more isotropically distributed as dictated by optimization procedures.

CONCLUSIONS

The variability of exposure (incurred radiation dose equivalent H) during a large solar particle event for an astronaut in a space habitation module is examined. A formal analytical development is presented that treats the dose equivalent fluctuations in terms of relevant thickness distributions and radiation spectral parameters. The general formalism is then applied to computerized geometric models of the human body in combination with a simulated space habitation module configuration. Calculation of average dose equivalent values and associated upper and lower bounds are illustrated dose equivalent-vs.-depth functions derived from observed large proton flare spectra. Computational cases considered include interior spacecraft locations that were heavily, moderately, and lightly shielded, with thickness distributions representative of conceptual future space habitation modules. Five target points within a geometric model of the human body were also considered in the analysis and typified varying degrees of body self-shielding.

In order to compare actual dose equivalent distribution functions with the theoretical means and bounds, statistical computations were performed for sets of random orientations of the various three-dimensional geometries. It was found that, in general, the actual, or practical, range of variability was substantially less than the absolute range. Examination of the data has indicated that an approximate realistic range may be obtained from the cumulative thickness distributions. Application of this technique could provide reasonable estimates of incurred dose equivalent variability with minimal computational effort for a wide variety of space exposure situations. Such analyses should considerably facilitate the further evaluation of estimated risks due to solar particle event exposures. It is recommended that the quantity $(\bar{H} + H_{\max})/2$ be used in shield-design studies to ensure that design exposure limits are rarely exceeded in actual practice.

REFERENCES

Atwell, W.; Weyland, M. D.; Simonsen, L. C. Solar particle dose rate build-up and distribution in critical body organs. In: Swenberg, C. E.; Horneck, G.; Stassinopoulos, E. G., eds. Biological effects and physics of solar and galactic cosmic radiation. New York: Plenum Press; 1993: 831–844.

Badhwar, G. D.; Cucinotta, F. A.; O'Neill, P. M. Depth-dose equivalent relationship for cosmic rays at various solar minima. Radiat. Res. 134:9–15; 1993.

Bertini, H. W.; Guthrie, M. P.; Culkowski, A. H. Nonelastic interactions of nucleons and π-mesons with complex nuclei at energies below 3 GeV. Oak Ridge, TN: Oak Ridge National Laboratory; Report No. ORNL-TM-3148; 1972.

Billings, M. P.; Yucker, W. R. The computerized anatomical man (CAM) model. Washington, DC: NASA; Report No. CR-134043; 1973.

Langley, R. W.; Billings, M. P. Methods of space radiation dose analysis with applications to manned space systems. Washington, DC: NASA; Report No. TM X-2440; 1972:108–116.

National Council on Radiation Protection and Measurements. Guidance on radiation received in space activities. Bethesda, MD: NCRP; Report No. 98; 1989.

Nealy, J. E.; Simonsen, L. C.; Wilson, J. W.; Townsend, L. W. Radiation exposure and dose estimates for a nuclear-powered manned mars sprint mission. In: Proceedings of the Eighth Symposium on Space Nuclear Power Systems. AIP Conf. 900116:531–536; 1991.

Schimmerling, W. Ground-based measurements of galactic cosmic ray fragmentation in shielding. Adv. Space Res. 12:445–459; 1992a.

Schimmerling, W. Radiobiological problems in space—An overview. Radiat. Environ. Biophys. 31:197–203; 1992b.
Shinn, J. L.; Wilson, J. W.; Nealy, J. E. Reliability of equivalent sphere approximation in blood forming organ dose estimation. Washington, DC: NASA; Report No. TM-4178; 1990.
Shinn, J. L.; John, S.; Tripathi, R. K.; Wilson, J. W.; Townsend, L. W.; Norbury, J. W. Fully energy-dependent HZETRN (a galactic cosmic-ray transport code). Washington, DC: NASA; Report No. TP-3243; 1992.
Smart, D. F.; Shea, M. A. Solar proton events during the past three solar cycles. J. Spacecraft Rockets 26:403–415; 1989.
Townsend, L. W.; Cucinotta, F. A.; Shinn, J. L.; Wilson, J. W. Effects of fragmentation parameter variations on estimates of galactic cosmic ray exposure—Dose sensitivity studies for aluminum shields. Washington, DC: NASA; Report No. TM-4386; 1992.
Wilson, J. W. Analysis and mechanization of three- and four-gimbal systems. Washington, DC: NASA; Report No. TN D-4689; 1968.
Wilson, J. W.; Khandelwal, G. S. Proton dose approximation in arbitrary convex geometry. Nucl. Technol. 23:298–305; 1974.
Wilson, J. W.; Khandelwal, G. S. Proton-tissue dose buildup factors. Health Phys. 31:115–118; 1976.
Wilson, J. W.; Townsend, L. W.; Badavi, F. F. Galactic HZE propagation through the earth's atmosphere. Radiat. Res. 109:173–183; 1987.
Wilson, J. W.; Townsend, L. W.; Nealy, J. E.; Chun, S. Y.; Hong, B. S.; Buck, W. W.; Lamkin, S. L.; Ganapol, B. D.; Khan, F.; Cucinotta, F. A. BRYNTRN: A Baryon transport model. Washington, DC: NASA; Report No. TP-2887; 1989.
Wilson, J. W.; Townsend, L. W.; Schimmerling, W.; Khandelwal, G. S.; Khan, F.; Nealy, J. E.; Cucinotta, F. A.; Simonsen, L. C.; Shinn, J. L.; Norbury, John W. Transport methods and interactions for space radiations. Washington, DC: NASA; Report No. RP-1257; 1991.
Wilson, J. W.; Nealy, J. E.; Schimmerling, W. Effects of radiobiological uncertainty on shield design for a 60-day lunar mission. Washington, DC: NASA; Report No. TM-4422; 1993a.
Wilson, J. W.; Nealy, J. E.; Wood, J. S.; Qualls, G. D.; Atwell, W.; Shinn, J. L.; Simonsen, L. C. Exposure fluctuations of astronauts due to orientation. Washington, DC: NASA; Report No. TP-3364; 1993b.

APPENDIX A

Optimum shield design

The environment in deep space can be assumed to be isotropic in most cases. One may represent the dose in a convex body as an integral of the dose in variable-radius spheres as

$$D(\vec{x}) = \int D_{sp}(r) f_b(r)\, dr, \tag{A1}$$

where we overestimate the dose in a sphere by dose in a slab. We consider a series of shapes with the same average thickness

$$\bar{t} = \int t\, f_b(t)\, dt, \tag{A2}$$

so we may ask which shape gives minimum exposure to the dose point. We model this question by assuming a class of distributions for the cardioid figure of rotation given as

$$F_b(t) = \begin{Bmatrix} 0 & t \le \bar{t} - \delta \\ (t - \bar{t} + \delta)/2\delta & (\bar{t} - \delta \le t \le \bar{t} + \delta) \\ 1 & \bar{t} + \delta < t \end{Bmatrix}, \tag{A3}$$

where $F_b(t)$ denotes the cumulative distribution function. We may then ask which of the doses for the areal density distribution given by eqn (A3) as a function of δ is least.

The dose in the center of a sphere decreases (approximately) as an exponential for most space radiations for which the dose in the cardioid figure becomes

$$D(\vec{x}) = D_{sp}(\bar{t}) \left(1 + \frac{1}{3!}\alpha^2\delta^2 + \frac{1}{5!}\alpha^4\delta^4 + \cdots\right), \tag{A4}$$

where α^{-1} is the e-folding distance of $D_{sp}(t)$. The dose within the shield increases monotonically with increasing δ and is minimum at $\delta = 0$, where the variation in δ is likewise zero. The optimum shield configuration is a sphere (spherical shell) whose radius is the mean thickness. Note that $D(\vec{x})$ changes rapidly with δ for $\delta > \alpha^{-1}$ but is relatively insensitive to changes in shape for $\delta < \alpha^{-1}$. Highly penetrating radiations (α small) are less sensitive to nonspherical shapes, while low penetration environments (α large) require δ to be small for optimum shielding.

It has been tempting in the past to assume that the dose at $\vec{x}$ can be estimated by the dose in the center of a sphere of the same average thickness. This point is further discussed by Langley and Billings (1972). Clearly, this is an under estimate for most practical problems and should be avoided, since astronaut exposure would always exceed design values. We may also conclude that the exposure is maximum in the center of a spherical-shell shield and decreases as one approaches the walls, since the minimum thickness is fixed and the average thickness increases as the wall is approached.

APPENDIX B

Rotation representations of astronaut orientation

This appendix gives the details of the relationship between the thickness distributions of dose points in the astronaut to the thickness distribution of the vehicle. The areal density about a point $\vec{x}$ is given as $t_x(\vec{\Omega})$ and is fixed to an astronaut reference frame for which aircraft standards are used (that is, $\hat{z}$ vertically down, $\hat{x}$ forward, and $\hat{y}$ out the right "wing"). The orientation angles will be taken as standard yaw (ψ), pitch (θ), and roll (ϕ). The areal density for the point $\vec{x}$ in the vehicle frame is then

$$t_x[R_x(\phi)R_y(\theta)R_z(\psi)\vec{\Omega}]. \tag{B1}$$

We represent the rotation operation in terms of directional cosines

$$\vec{\Omega}_y = R_x(\phi)R_y(\theta)R_z(\psi)\vec{\Omega}, \tag{B2}$$

where R represents the usual rotation matrices (Wilson 1968). The three angles can be chosen for a fixed astronaut orientation or represented through statistical sampling for which uniform distributions are used as

$$\psi \in U(0, 2\pi), \cos\theta \in U(-1, 1) \text{ and } \phi \in U(0, 2\pi). \tag{B3}$$

Future work will examine the statistical fluctuations of organ doses for an astronaut in a habitat such as space station *Freedom*.

■ ■